4.0 ANALYSIS OF AIRCRAFT OBSERVATIONS

Anna Karion, Sam Oltmans, Gabrielle Pétron, Colm Sweeney, and Russ Schnell

NOAA/GMD and CU/CIRES

4.1 Introduction and Methodology

During the UBOS 2013 campaign, a single-engine Cessna 210 aircraft (owned and operated by Kalscott Engineering, www.kalscott.com) was deployed in the Uinta Basin by NOAA Global Monitoring Division's (GMD) aircraft program. Instruments drew air through dedicated inlets installed under the aircraft's starboard wing (Figure 4-1). On-board instrumentation included high-frequency analyzers for carbon monoxide (CO), carbon dioxide (CO_2), methane (CH_4), and water vapor (H_2O) (Picarro G2401m), nitrous oxide (NO_2) (Los Gatos Research), and ozone (O_3) (2B Systems). NOAA's custom flask packages were used to collect discrete air samples over the Uinta Basin and sent back to NOAA for analysis of 50+ trace gases, including CO, CO_2, CH_4, and light hydrocarbons such as C_3H_8 (propane), n-C_4H_{10} (butane), i- and n-C_5H_{12} (pentane), C_2H_2 (acetylene), C_6H_6 (benzene). The same air samples were then analyzed for additional hydrocarbons, including heavier compounds, at the Institute of Arctic and Alpine Research (INSTAAR) at the University of Colorado. GPS location and time information, temperature, relative humidity, and ambient pressure measurements were also collected onboard and synchronized with the ambient mole fraction measurements. Measurements of trace gases both from the in-situ continuous analyzers (except for O_3 and NO_2) and the flask packages are all reported on the NOAA/WMO calibration scales as dry air mole fractions (moles per mole of dry air), using methods outlined in Karion et al. (2013) and online at http://www.esrl.noaa.gov/gmd/ccgg/aircraft/packages.html. The 2B UV photometric O_3 analyzer was calibrated against a NOAA/GMD maintained standard that is regularly compared with a U.S. NIST standard and compared with the NOAA/GMD standard before and after the campaign. Measurements of NO_2 have an internal instrument "zero cycle" calibration but are not otherwise calibrated.

(a) (b)

Figure 4-1. Photographs of the Cessna 210 aircraft that sampled over the Uinta Basin in February 2013. (a) Three inlets and two temperature and humidity probes were installed under the starboard wing. (b) View of the snow covered Uinta Basin from the aircraft.

Seven flights were conducted over an 8-day period from January 31 to February 7, 2013. During this time snow-covered ground, low surface temperatures, low wind speeds and minimal cloud cover all provided excellent conditions for a temperature inversion that trapped surface emissions within the topographic boundaries of the Uinta Basin. Pollutants emitted at the surface within the basin were essentially trapped in a shallow boundary layer up to approximately 1650±50 meters above sea level (masl) (100-200 meters above ground level (magl), depending on the elevation). Research flights surveyed the region, generally flying either at low altitude within the mixed surface layer and the inversion layer or dipping in and out of the inversion layer. Flights were conducted during a multi-day episode of ozone pollution at the surface to characterize some of its spatial and temporal features.

During the 8-day period over which the aircraft flights were conducted, surface ozone built up from approximately background levels of 60 ppb to over 130 ppb. The distribution of O_3 during the flight of February 2, 2013 is shown in Figure 4-2 along with a depiction of the terrain in the basin. The first flight on January 31 occurred after the basin had been flushed out by the passage of a frontal system three days earlier. The final flight on February 7 took place just prior to the passage of another weather disturbance that again led to the flushing of ozone and related gases measured by the aircraft, bringing concentrations back to near background levels. The buildup and dispersal of ozone and related constituents across the basin are captured in the seven flights over the 8-day period.

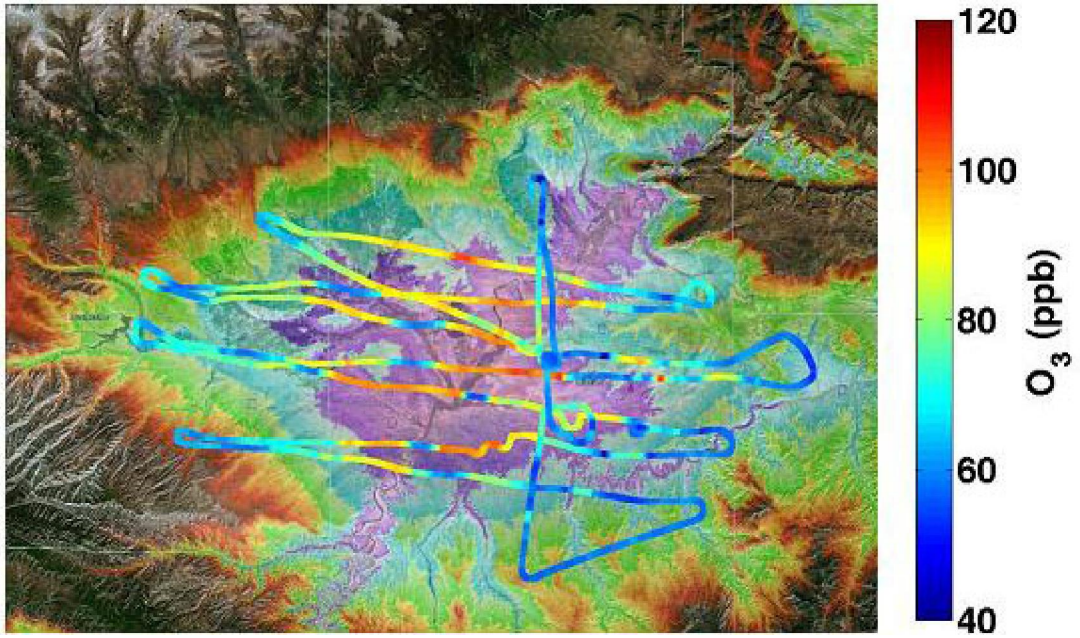

Figure 4-2. Flight tracks over the Uinta Basin on February 2, 2013 colored by O_3 mole fraction in parts per billion (ppb). Data from all altitudes is shown overlain on topography of the Uinta Basin. The 1600 m elevation is at the boundary between the purple and turquoise color band.

Section 4.2 details the spatial distribution of CH_4, CO, CO_2, and NO_2 through the basin and their interrelationships, Section 4.3 presents the characteristics of ozone measured through the basin and relationships with the other measured constituents and Section 4.4 presents the vertical distribution of ozone and the other constituents. Data from the airborne flask sampling, including measurements of volatile organic compounds (VOCs), are presented in Section 4.5.

4.2 Spatial Distribution of CH_4, CO, CO_2, and NO_2

The spatial distributions of CH_4, CO, CO_2, and NO_2 within the shallow boundary layer were investigated during the campaign. Figure 4-3 shows the distribution of CH_4 (a,c) and CO (b,d) measured over the Uinta Basin on February 2, 2013. Panels (c) and (d) only show data collected below 1650 masl (i.e. within the shallow mixed boundary layer) on that day. The measurements in the mixed surface layer indicate that CH_4 and CO are not as evenly distributed in the basin as O_3 (see Section 4.3). We infer that low and variable winds during the inversion conditions inhibited vigorous horizontal mixing, so that the emissions of these species did not advect far from their original source. Horizontal wind measurements by high-resolution Doppler lidar (HRDL) at Horsepool support this conclusion: during the period from February 1 to February 7 surface winds were low (averaging between 1-1.5 m/s in the boundary layer) and changing direction, so that horizontal transport of emissions within the basin was minimal.

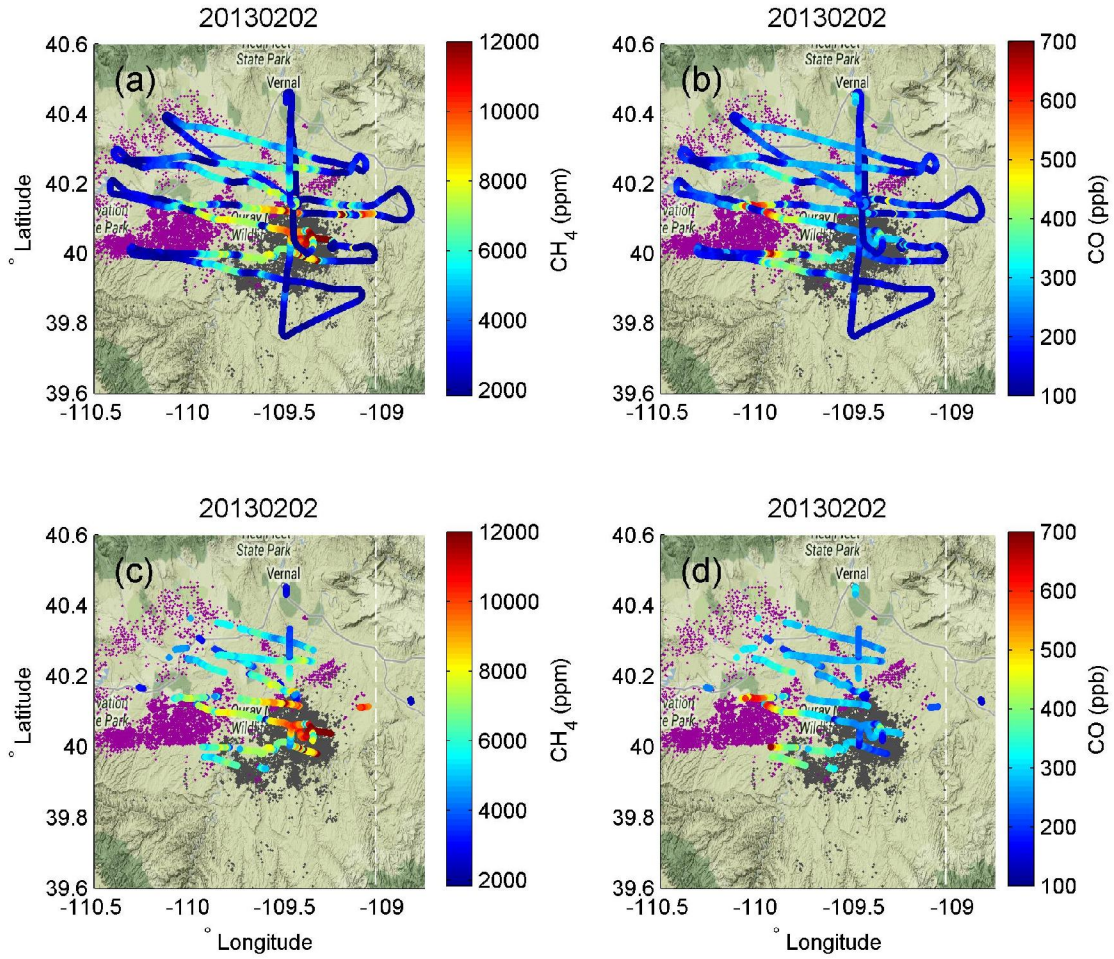

Figure 4-3. Map of the flight track on February 2, 2013 over the Uinta Basin colored by (a,c) CH_4 and (b,d) CO. Figures (a) and (b) show the full track, while (c) and (d) show the flight track portions below 1650 masl only. Locations of oil and gas wells are shown as purple and gray dots, respectively.

To analyze the extent of trace gas enhancements and their differences across the various regions of the basin, the flight tracks were separated into four quadrants: South-East (SE), South-West (SW), North-West (NW) and North-East (NE). Trace gas observations from each quadrant were colored differently and correlations between the different species for altitudes below 1650 masl were investigated (Figure 4-4).

An analysis of the measurements collected on February 2, 2013 shows elevated CO in the SW quadrant relative to all the other species and relative to the other quadrants. In the SE, CH_4 is enhanced more per unit CO than in the SW, while in the SW, more CO is generated per unit CH_4 (Figure 4-4c). In the SW, more CO is generated per unit CO_2 as well, indicating a potential source with inefficient combustion emissions in that area. The enhancement ratio of CO to CO_2 in the SW (green in Figure 4-4(b)) is significantly greater than those reported in the literature

for either direct tailpipe vehicular emissions (9-18 ppb CO per ppm CO_2 ([Bishop and Stedman, 2008]) or urban areas (10-14 ppb CO/ppm CO_2, [Miller et al., 2012; Peischl et al., 2013; Turnbull et al., 2011; Wunch et al., 2009], black lines in Figure 4-4(b)). The measurements shown in Figure 4-4 do not include data points taken within the power plant plume; that plume was present above the 1650 masl layer as will be discussed in Section 4.4.3. However, we note here for later reference that the power plant plume shows correlations of 6-10 ppb CO per ppm CO_2 (not shown), consistent with the solid and dashed black lines in Figure 4-4(b). The relatively larger enhancements of CO in the SW quadrant and enhancements of CH_4 in the SE are present in all flights; Figure 4-5 shows the CO to CH_4 and CO to CO_2 correlations for all seven flights in 2013.

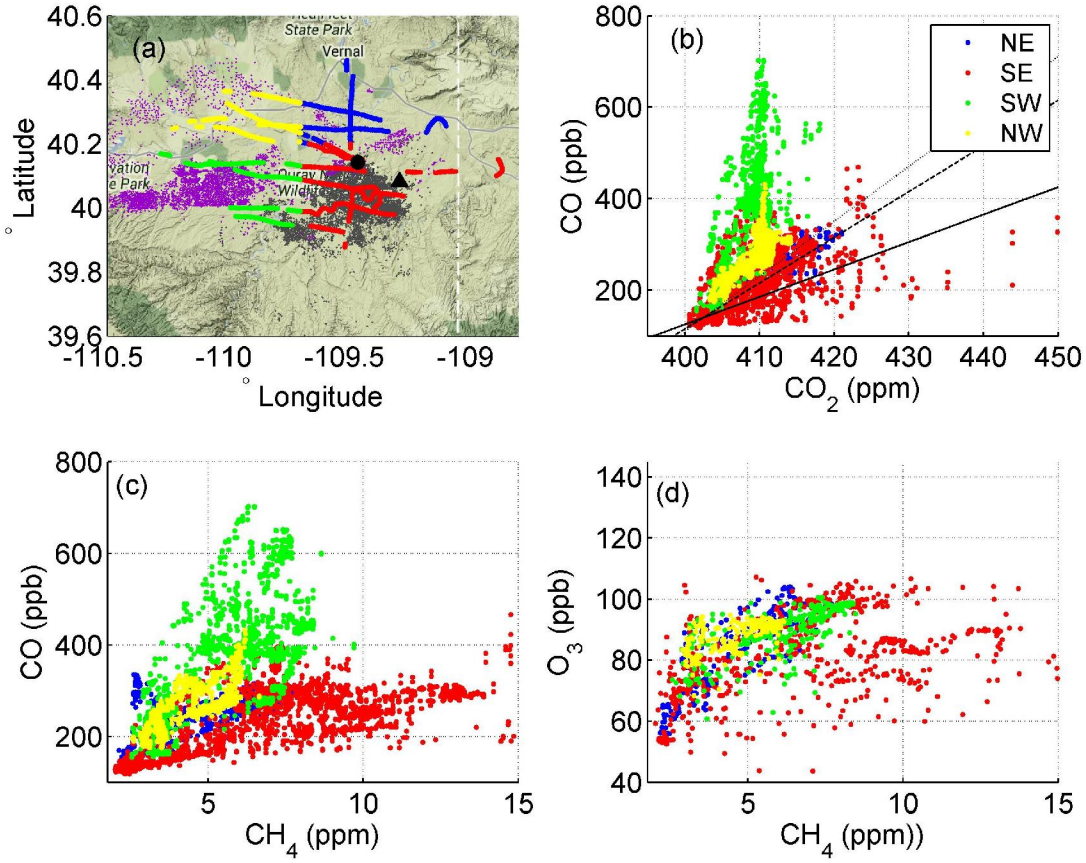

Figure 4-4. Spatial analysis of trace gas dry air mole fraction correlations during the February 2, 2013 flight. (a) Map of the flight track below the inversion (1650 masl) colored by quadrant (red: SE, blue: NE, yellow: NW, green: SW). The location of Horsepool is noted with a black circle; the Bonanza power plant is a black triangle; gas wells are in gray; oil wells are in purple. (b) Correlation plot of CO with CO_2 in the four quadrants. Black dotted line shows a molar ratio of 12 ppb CO per ppm of CO_2, dashed line is 10 ppb per ppm, and solid line is 6 ppb/ppm. (c) Correlation plot of CO with CH_4, indicating more CO emission per unit CH_4 in the SW quadrant, and more CH_4 per unit CO in the SE. (d) Correlations of CH_4 with O_3 show less spatial separation, supporting the observation that O_3 is observed more uniformly through the region.

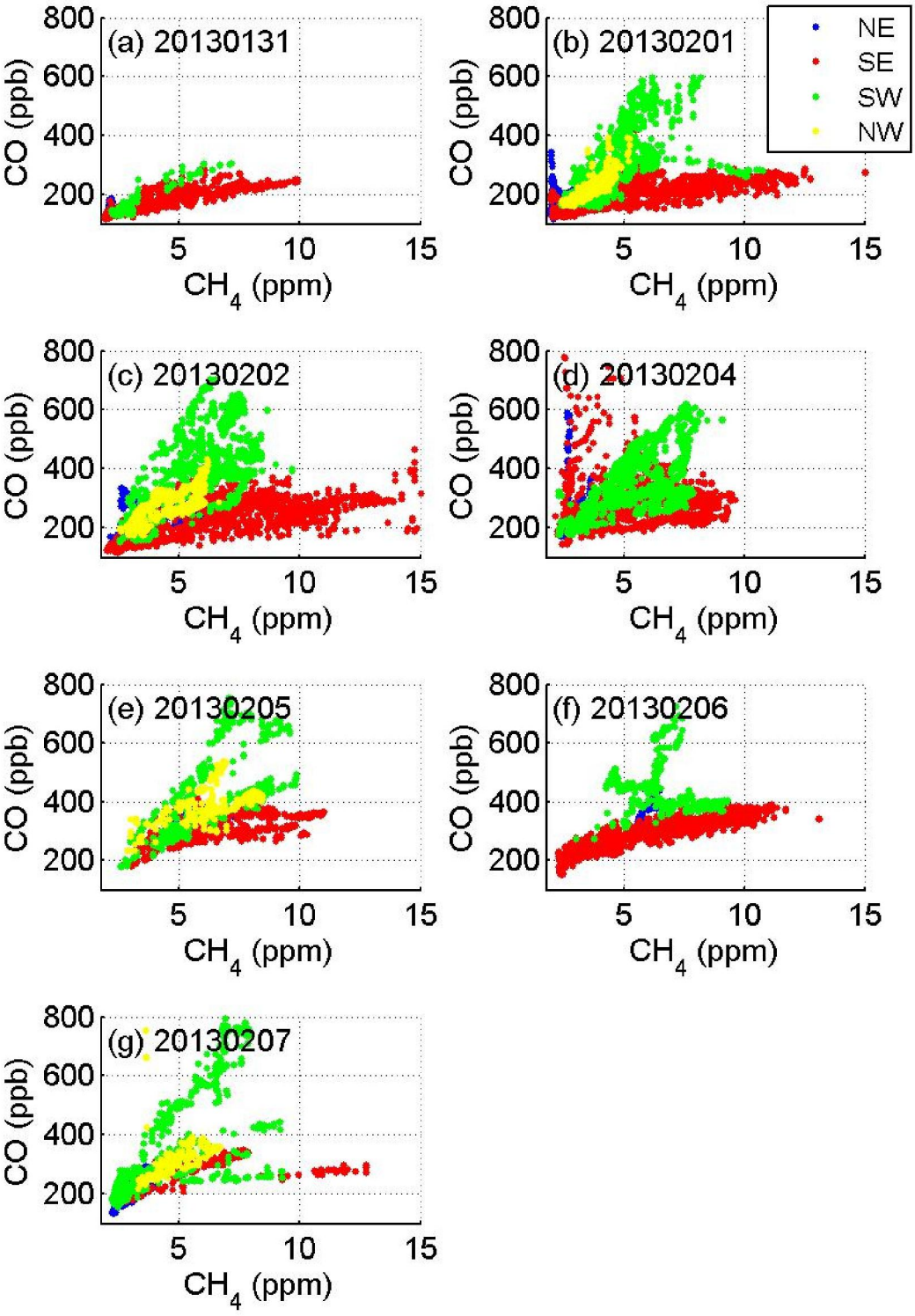

Figure 4-5. Correlations of CO with CH_4 over the different quadrants of the basin for the seven flights, with the flight date indicated in each panel (YYYYMMDD).

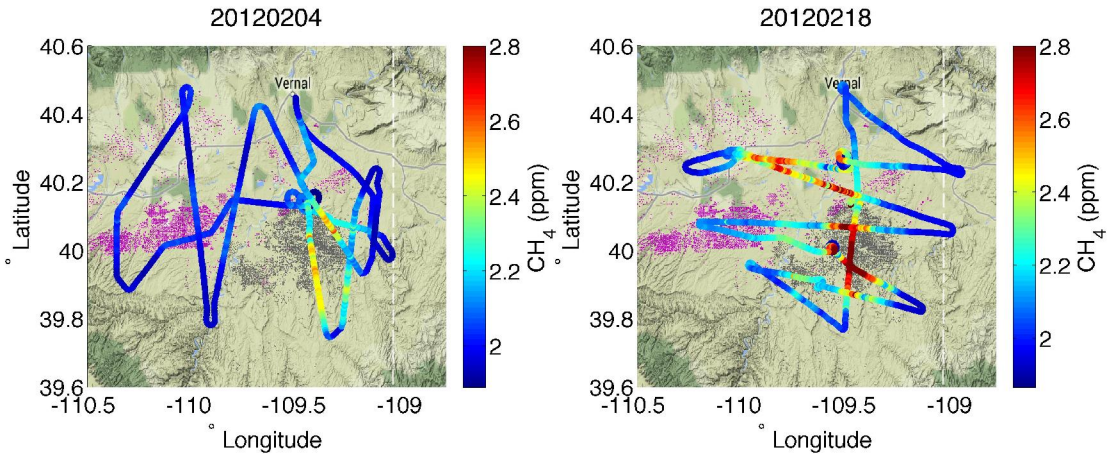

Figure 4-6. Flight tracks from (a) February 4 and (b) February 18, 2012 showing elevated CH_4 over the gas wells (gray dots) during low-wind conditions, in the same region that CH_4 was enhanced in the 2013 flights, with lower enhancements in the western portion of the basin over the oil wells (purple dots).

Based on ground measurements from the NOAA mobile laboratory in 2012 that showed high CO to CO_2 and CO to CH_4 emissions ratios from pump-jack engines in the oil field, we suspect that emissions from inefficient combustion of the pump-jack engines in the SW portion of the basin may be the cause of the large CO mole fractions observed there. An oil rig fire in the NW quadrant of the region (40.36 N, -110.01 W) that started on January 22, 2013 was likely still an emissions source until it was out fully on February 6, and may have also influenced the aircraft measurements. However, the NW quadrant does not show CO as elevated as the CO measured in the SW, so we do not believe that the fire was the primary source of the CO enhancements observed farther south.

On most days, CH_4 mole fractions are lower in the NW and SW quadrants than in the SE, showing that the gas field in the southern part of Uintah County has higher CH_4 mole fractions than the oil field. This was also observed in flights conducted the previous year, in February 2012 (Figure 4-6), indicating that a significant portion of CH_4 emissions in this quadrant is likely persistent. Possible CH_4 emission sources in the SE quadrant include a dense array of compressor stations and two processing plants (the Chipeta Plant Complex and Stagecoach/QEP); there is also a large density of natural gas-production wells in the area as well, so the exact mix of sources and their relative contribution are still unknown.

Although NO_x are mainly emitted from combustion sources (just as CO is), the most elevated NO_2 is not observed in the same region as the elevated CO (Figure 4-7 shows correlations of NO_2 to CO for the different quadrants). In the flight data, NO_2 mole fractions are highest in the same SE region as the elevated CH_4, although it is not well correlated with CH_4 (Figure 4-8). Based on the flight data, it appears that the formation of NO_2 is occurring preferentially near the processing plants and compressor stations in the SE quadrant. Additional analysis of the chemistry and horizontal transport is needed to confirm this conclusion.

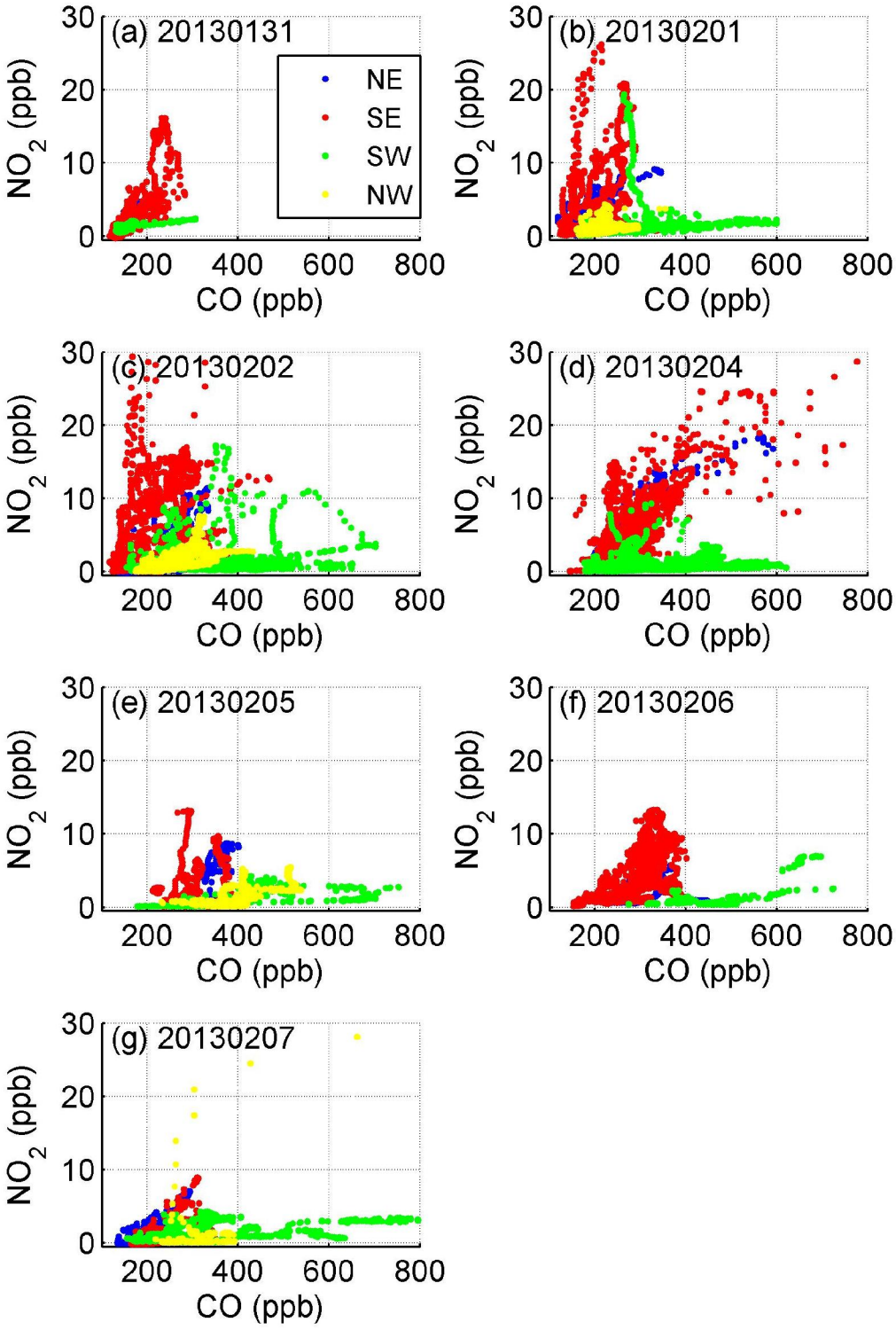

Figure 4-7. Relationship between NO_2 and CO measurements from the aircraft for different quadrants in the basin (date of flight indicated in each panel, YYYYMMDD). NO_2 is more enhanced in the SE, while CO is enhanced in the SW.

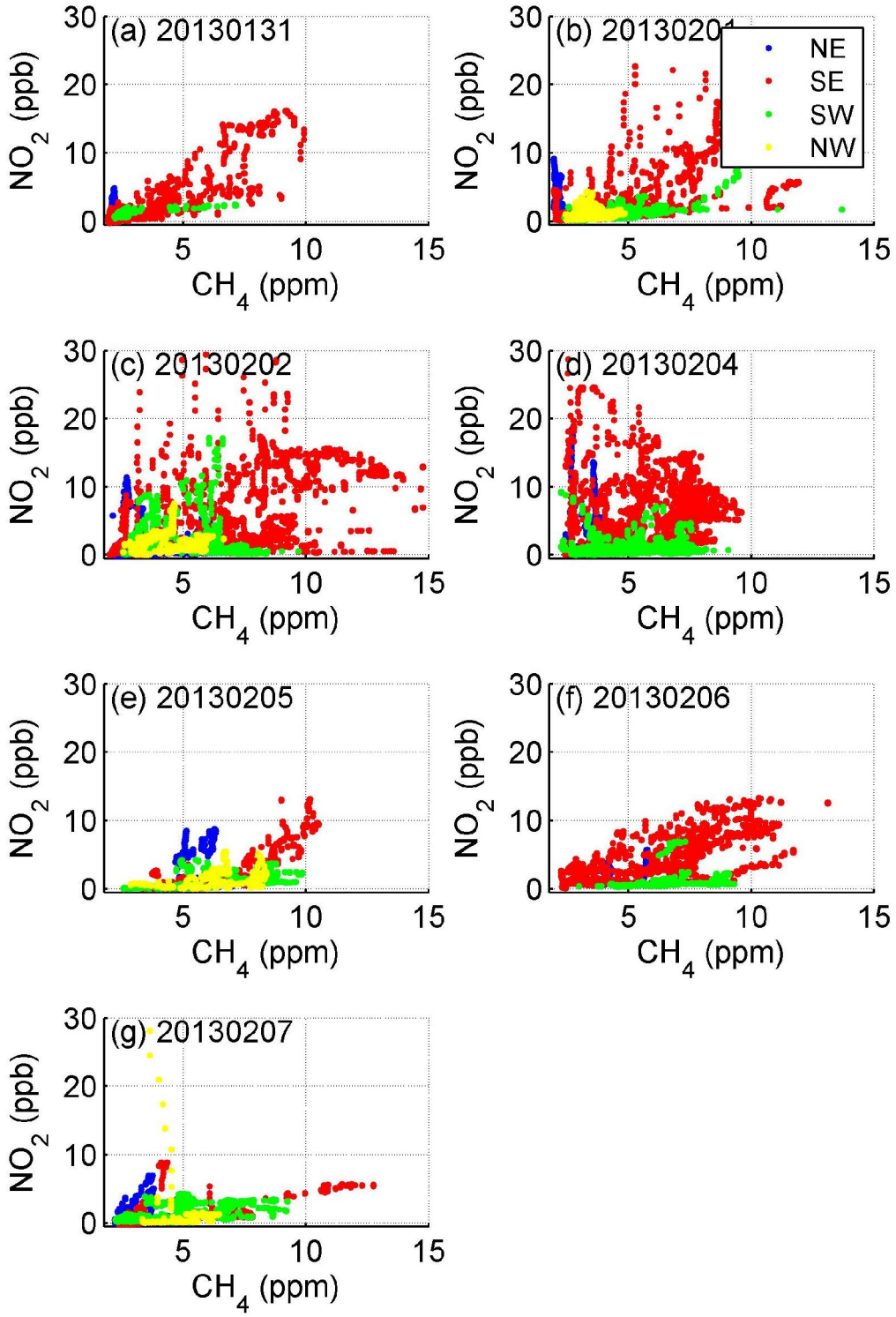

Figure 4-8. Relationship between NO_2 and CH_4 measurements from the aircraft for different quadrants in the basin (date of flight indicated in each panel, YYYYMMDD). NO_2 and CH_4 are both enhanced in the SE quadrant (red points), but not always well-correlated.

4.3 Spatial Distribution of Ozone and Relationship to Other Constituents

As a secondary pollutant the distribution of ozone both spatially (horizontal and vertical) and temporally reflects photochemical production and loss involving precursor emissions, dispersal of these emissions within the basin and redistribution of ozone due to air motions within the basin. Both the VOC and NOx sources are not uniformly distributed over the Basin but are generally strongest in the SE sector (in Uintah County) where the major gas field is located. This is seen in the elevated levels of methane (Figures 4-3(c) and 4-5) and the accompanying non-methane hydrocarbons that strongly correlate with methane (Figures 4-22 and 4-23 in Section 4.5). Although the NO_2 measurements on the aircraft are not a direct measurement of the emitted NO, the high NO_2 amounts over the SE sector (Figures 4-7 and 4-8) indicate that there is a significant local NO source through the strong interrelationship between NO and NO_2 ($NO + O_3 \rightarrow NO_2 + O_2$ and $NO_2 + h\nu \rightarrow NO + O$).

4.3.1 Distribution of Ozone over the Uinta Basin

The distribution of ozone across the basin for flights between January 31 and February 6 below 1650 masl is shown in Figure 4-9 (flights on February 7 did not cover a significant portion of the basin). Several key features should be noted. There is a continuing buildup in the highest ozone concentrations through the progression of the flights. On January 31, O_3 mixing ratios over most of the basin are less than about 70 ppb with values near 80 ppb in the SE sector. By February 1 ozone is already >80 ppb over much of the basin and the high values are not confined to the SE. This pattern continues as ozone builds throughout the course of the week, reaching values in excess of 130 ppb. The flights on February 1 and 2 have the most extensive coverage of the basin below 1650 masl and very clearly show that high ozone is ubiquitous throughout the basin. The aircraft flight times in the afternoons are representative of the ozone resulting from the daytime photochemical production.

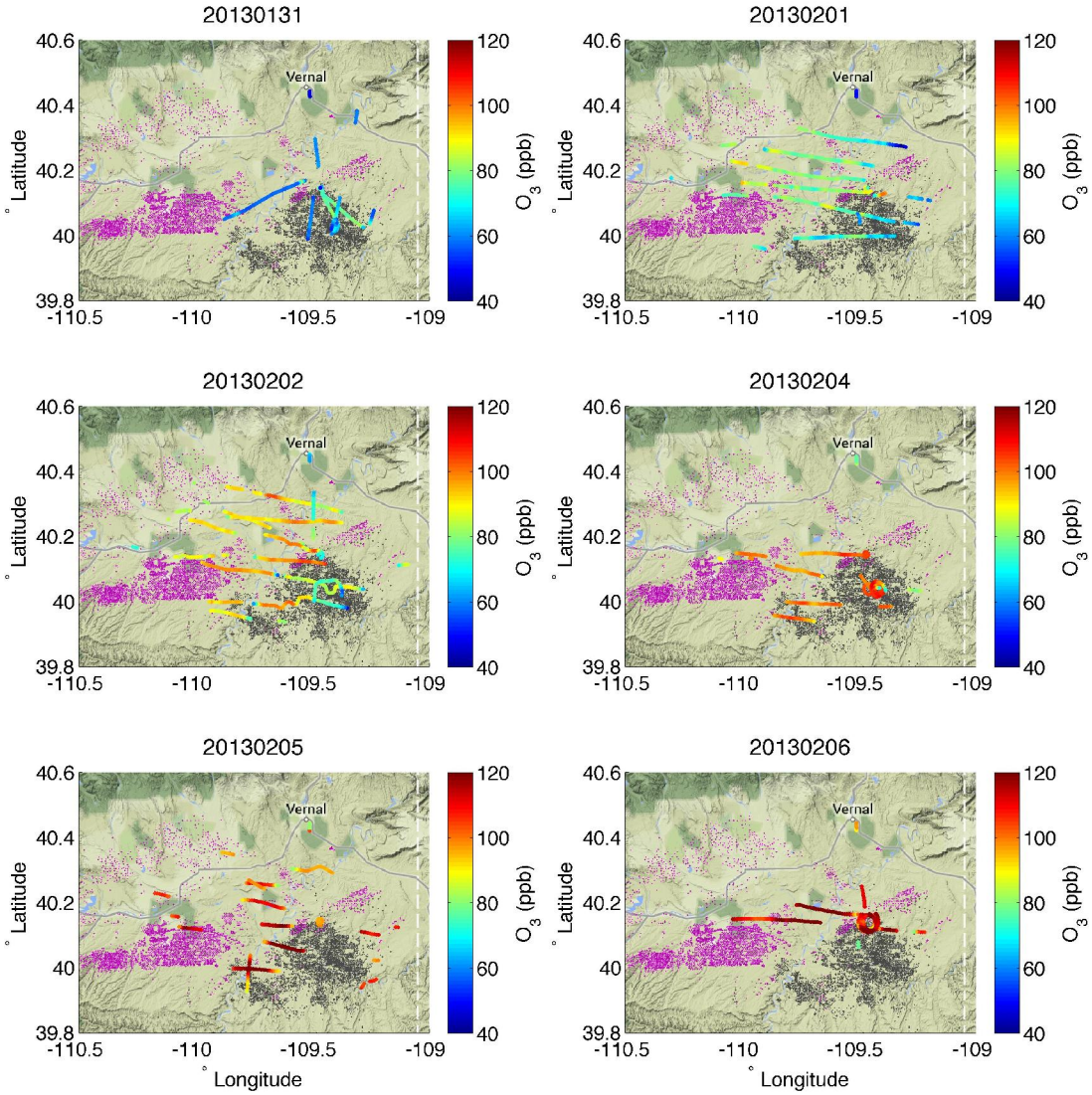

Figure 4-9. Map of flight tracks below 1650 masl on January 31, February 1, 2, 4, 5 and 6, 2013 over the Uinta Basin colored by O_3 mixing ratio in ppb. The flight date (YYYMMDD) is indicated in the title of each panel. Oil wells are indicated by purple points, gas wells by dark gray points.

4.3.2 Relationship of Ozone to Other Constituents Measured on the Aircraft

Though CH_4 values (and accompanying non-methane hydrocarbons including ozone precursor VOCs) are highest near the gas fields in the SE sector (Figure 4-3(c)), high CH_4 values and high coinciding NMHC mole fractions in discrete air samples are seen across the basin indicating a high potential for ozone production.

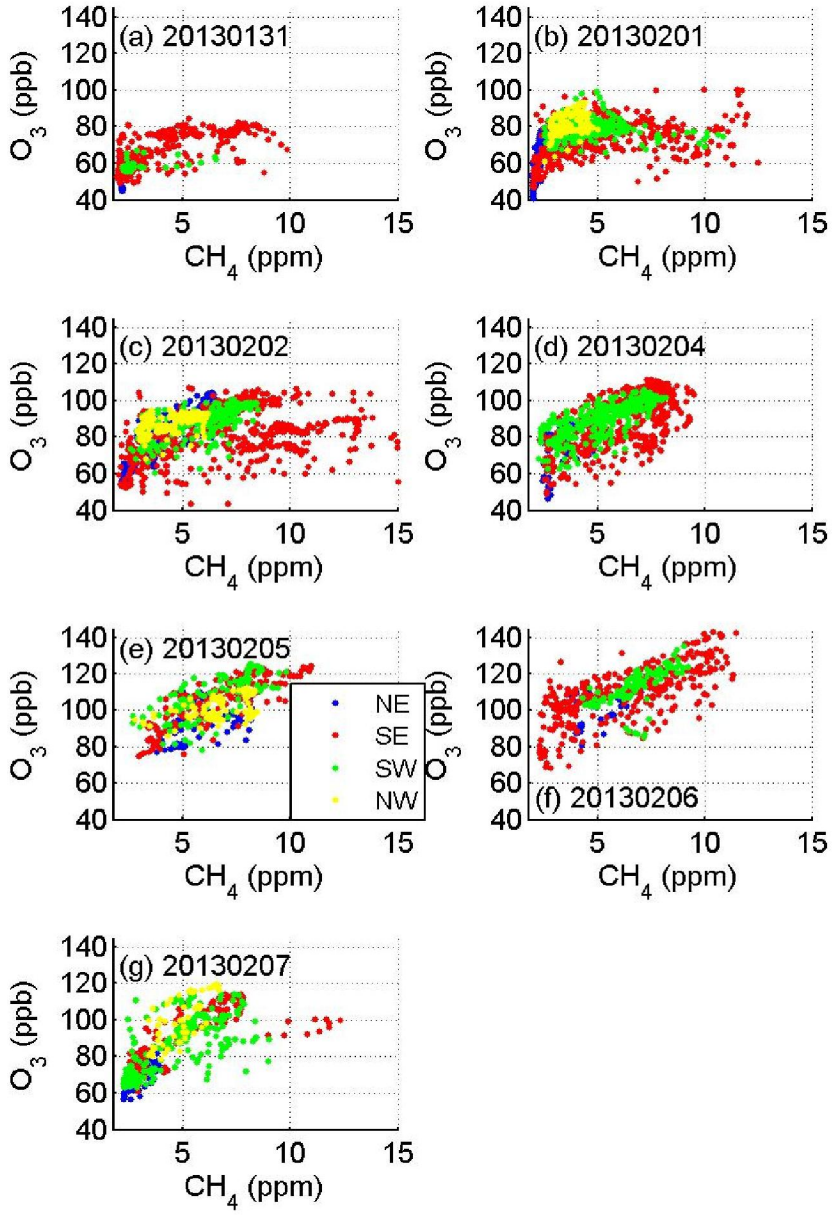

Figure 4-10. Relationship between O_3 and CH_4 measurements from the aircraft for different quadrants in the basin (date of flight indicated in each panel, YYYYMMDD). CH_4 is highest in the SE quadrant (red points), but is not well-correlated with O_3 for CH_4 above ~8 ppm.

In general ozone amounts increase with increasing methane although for the very highest methane values (>8 ppm), seen primarily in the SE sector where the primary gas field is located, this is not the case, especially when peak ozone values are <100 ppb (Figure 4-10). The relationship between ozone and methane appears similar throughout the basin with the exception of the very high methane in the SE.

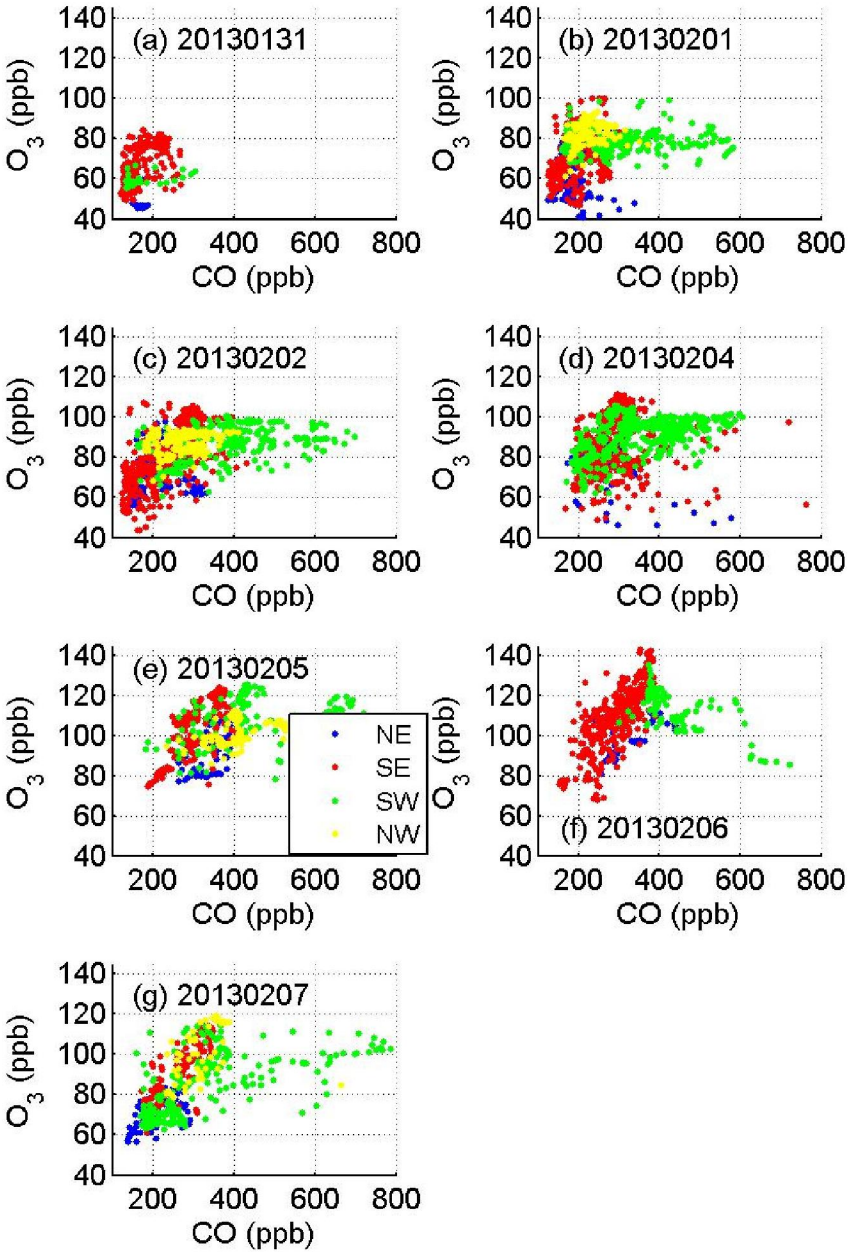

Figure 4-11. Relationship between O_3 and CO measurements from the aircraft for different quadrants in the basin (date of flight indicated in each panel, YYYYMMDD). CO is highest in the SW quadrant (green points), but is not well-correlated with O_3 for CO above 400 ppb.

In the NO_x-VOC dominated ozone production chemistry in the Uinta Basin, CO has a lesser role as an ozone precursor but may be indicative of a combustion source that also emits NO. Figure 4-11 shows a general increase in ozone with increasing CO. The most anomalous feature is the very large CO values in the SW sector that do not correlate with ozone. These much higher CO values in the SW are apparent in the relationship with all the trace gases measured on the aircraft including CH_4, CO_2, and NO_2 (see Figures 4-6).

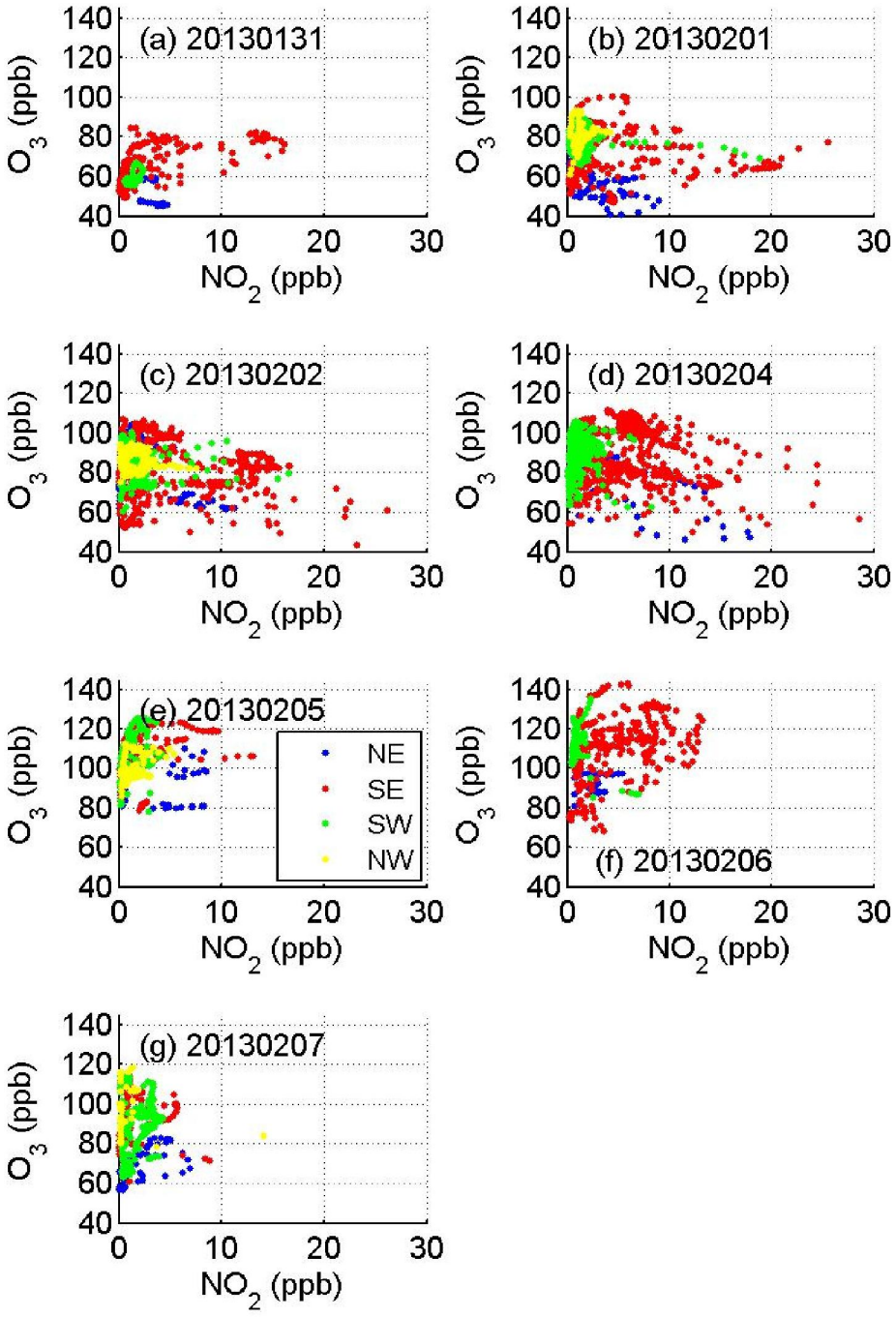

Figure 4-12. Relationship between O_3 and NO_2 measurements from the aircraft for different quadrants in the basin (date of flight indicated in each panel, YYYYMMDD). NO_2 is consistently highest in the SE quadrant (red points), but is not well-correlated with ozone.

As noted earlier, NO_2 is photochemically interrelated with O_3 and NO but is not expected to maintain a conservative relationship with O_3. As can be see seen in Figure 4-12, O_3 and NO_2 are not well correlated. While occasional values of NO_2 >5 ppb are seen in all of the sectors, this level is regularly seen in the SE sector (red points) suggesting this is an area of NO emissions.

With this sector also a strong source of CH_4 (although CH_4 is not always well-correlated with NO_2 as noted earlier – see Figure 4-8) and with the strong source of accompanying non-methane hydrocarbons, this sector dominated by the gas field operations appears to be the focal point for the precursor emissions responsible for ozone production in the Uinta Basin.

4.4 Vertical Distribution of Ozone and Other Constituents

During each of the seven aircraft flights in 2013, the aircraft conducted two or more vertical profiles, in which measurements were collected either in a spiral ascent or descent, or during an ascent/descent that also transited horizontally. Data collected during these profiles are valuable in assessing the extent of vertical mixing within the inversion layer, quantifying the gradient in mole fractions of species above and within the layer, and observing features that exist entirely above the inversion layer. They also illustrate the ozone buildup over several days within the lowest portion of the profiles.

4.4.1 Mixing within the Inversion Layer

Aircraft vertical profiles (Figures 4-13 - 4-19) generally show that the various trace gases are strongly enhanced and sometimes well-mixed below the height of the inversion. This altitude varied slightly depending on location within the basin, day, and time of day, but was generally at 1650±50 masl. Figure 4-13 shows a vertical profile conducted on January 31 over the ground site at Horsepool, in the north of the natural gas field (see Figure 4-14(b)). Figure 4-14 shows the timing (a) and location (b) of the profiles on February 1 that have been selected and shown in Figure 4-15. Figures 4-16 - 4-17 and 4-18 - 4-19 are the same as Figures 4-14 - 4-15, but for the flights of February 2 and 5, 2013.

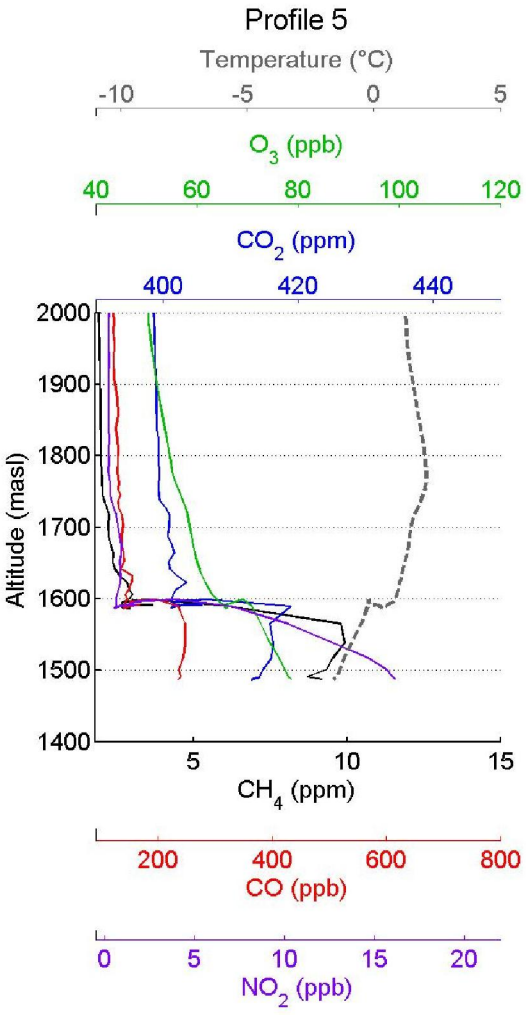

Figure 4-13. Profiles of constituents measured on the aircraft on January 31 in the vicinity of the natural gas field and gas processing plants. Note the enhancements of all species beneath the temperature inversion observed at 1600 masl.

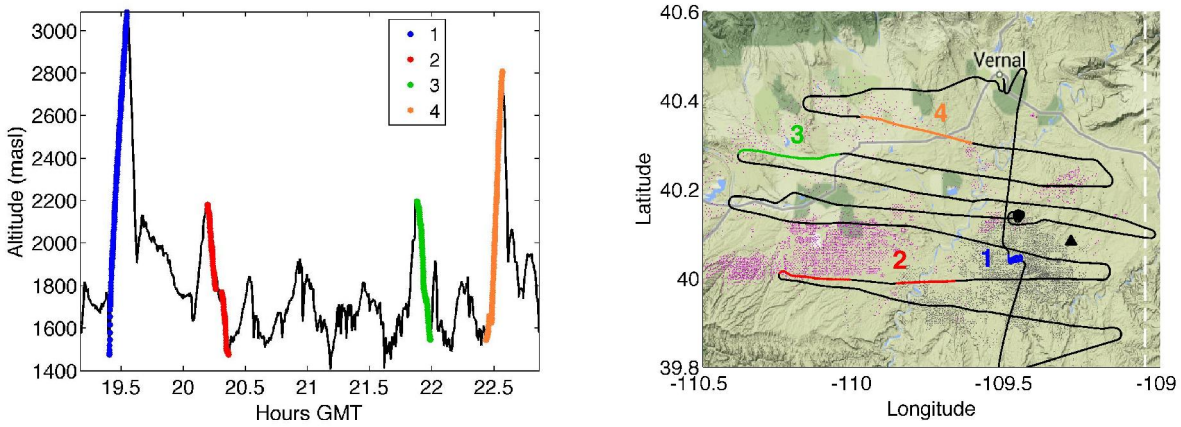

Figure 4-14. (a) Time series of flight on February 1, 2013, with the profiles highlighted. (b) Corresponding locations of the profiles in the Uinta Basin, shown along with the oil (purple) and gas (gray) well locations. The Bonanza Power Plant is located at the black triangle and Horsepool at the black dot.

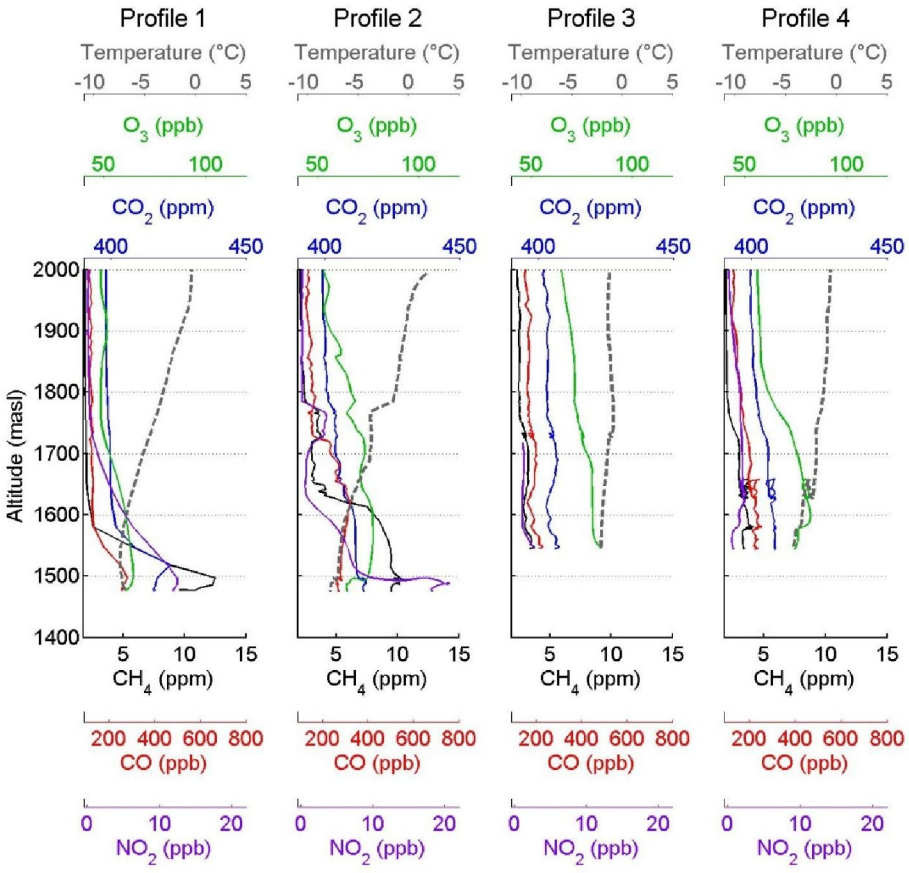

Figure 4-15. Four vertical profiles of CH_4 (black), CO (red), CO_2 (blue), O_3 (green), NO_2 (purple), and temperature (gray dashed) on February 1, 2013. Profile times and locations are indicated in Figure 4-14.

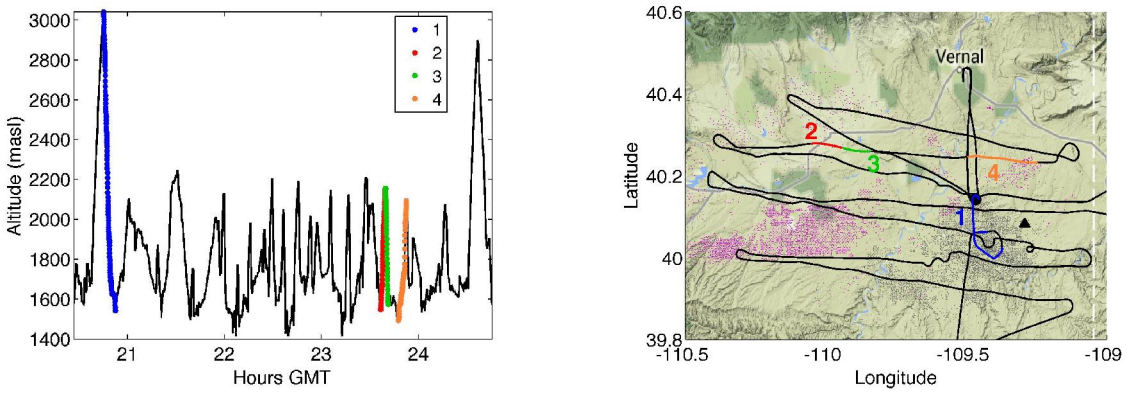

Figure 4-16. (a) Time series of flight on February 2 2013, with the vertical profiles highlighted. (b) Corresponding locations of the profiles in the Uinta Basin, shown along with the oil (purple) and gas (gray) well locations. The Bonanza Power Plant is located at the black triangle close to the blue numeral 1. Profile 4 is located over the ground site in Horsepool.

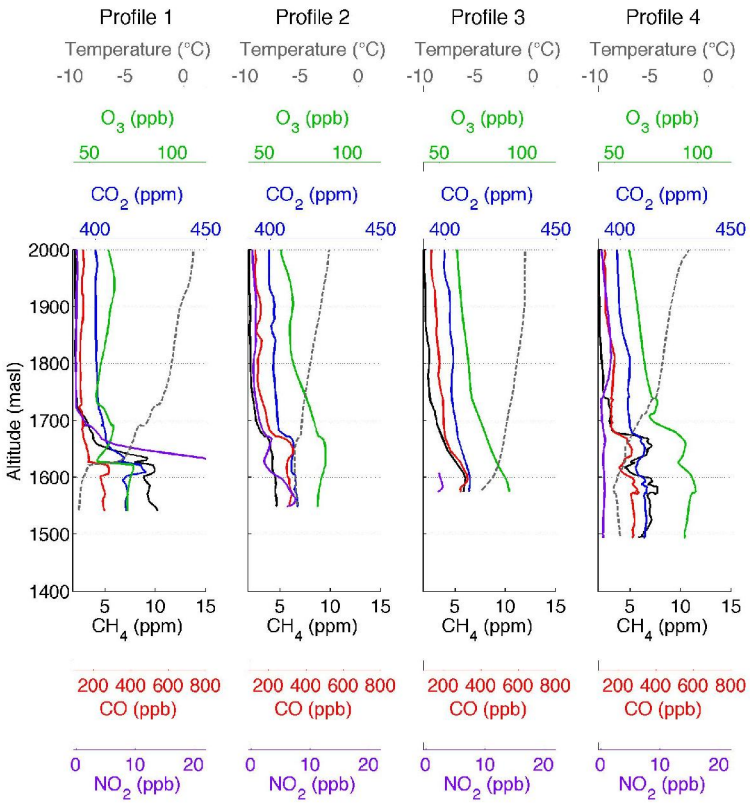

Figure 4-17. Four vertical profiles of CH_4 (black), CO (red), CO_2 (blue), O_3 (green), NO_2 (purple), and temperature (gray dashed) on February 2, 2013. Profile times and locations are indicated in Figure 4-16.

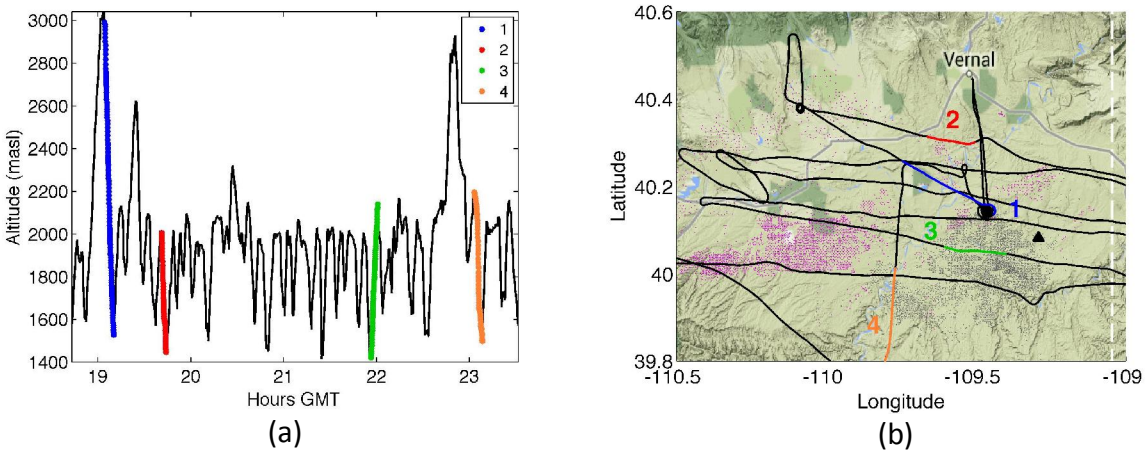

Figure 4-18. (a) Time series of flight on February 5 2013, with the profiles highlighted. (b) Corresponding locations of the profiles, shown along with the oil (purple) and gas (gray) well locations. The Bonanza Power Plant is located at the black triangle. Profile 1 was conducted near the Horsepool site.

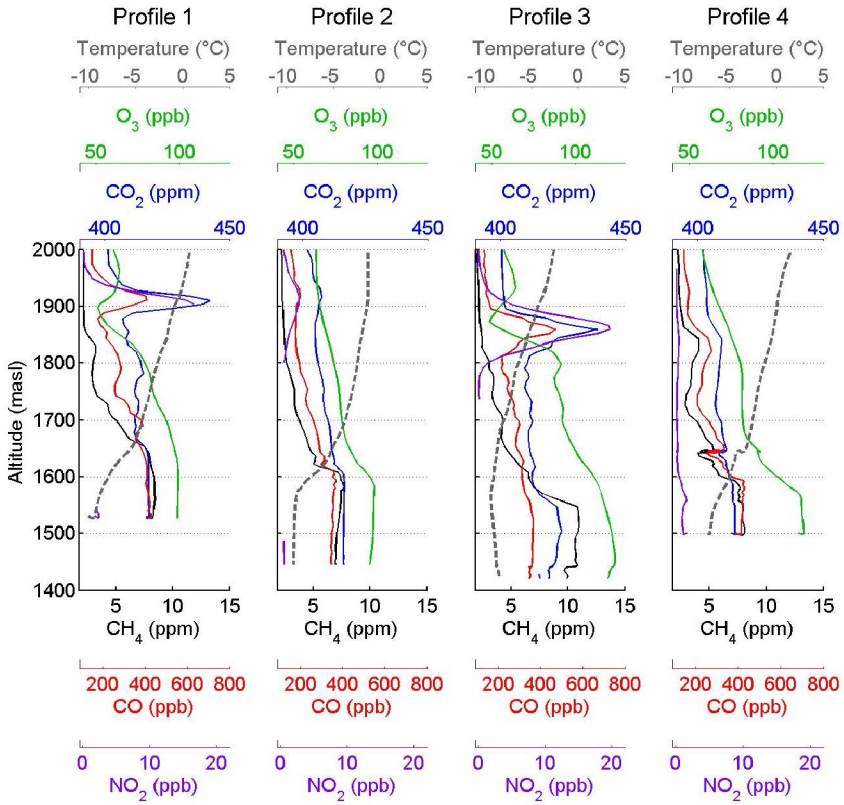

Figure 4-19. Four vertical profiles of CH_4 (black), CO (red), CO_2 (blue), O_3 (green), NO_2 (purple), and temperature (gray dashed) from the flight on February 5, 2013. Profile times and locations are indicated in Figure 4-18.

Most vertical profiles after January 31 (Figures 4-15, 4-17, and 4-19) illustrate the sharp gradient observed in most of the trace gases, generally at altitudes of 1600-1700 masl; the location of the trace gas mole fraction gradients generally corresponds to the altitude of the strongest gradient in temperature. Below this gradient, O_3, CH_4 and other constituents are almost always clearly enhanced above their free-tropospheric values.

4.4.2 Ozone Vertical Structure

Details on the vertical structure of ozone and particularly the way in which the buildup of ozone takes place with height is best captured with the three tethered ozonesonde sites (Ouray, Fantasy Canyon, and Horsepool) and the ozone lidar at the Horsepool location. These results are discussed in other sections of this report. The vertical profiles obtained on the aircraft flights provide vertical detail on the relationship of ozone with the other measured constituents. The profiles also show how ozone and the other gases are distributed in the vertical across the basin and particularly the differences near the gas field with large precursor sources.

The structure of the profiles has significant variations both in the vertical and spatially in the Basin. Profiles on February 1 (Figures 4- 14 - 4-15), February 2 (Figures 4-16 - 4-17), and February 5 (Figures 14-8 - 4-19) capture many of the important features seen in the aircraft profiles. The limited sampling below 1650 masl on January 31 (see Figure 4-9) shows only a small buildup of ozone and other constituents in the layer below 1650 masl in the SW sector or to the north and south of the gas field (not shown). In the heart of the gas field (Figure 4-13) there was a well-mixed layer below ~1600 masl with enhanced ozone (~80 ppb), and CO (~300 ppb), and very high CH_4 (~10 ppm) and NO_2 (~15 ppb near the surface). This is an indication that emissions from the gas field were building after the flushing of the basin that took place three days earlier (based on measurements from surface and ozonesonde observations) and significant ozone production was occurring, but was not generally widespread over the basin.

On February 1 flights covered a large portion of the basin and vertical profiles were conducted both in the gas field and well away from the field (Figures 4-14 - 4-15). Profile 1 in Figure 4-15 was carried out in the heart of the gas field (Figure 4-14). The top of the lowest inversion is only at about 1550 masl. Very high levels of CH_4 and NO_2 are confined beneath this shallow inversion. Ozone is only modestly elevated in mixing ratio (approximately 10-40 ppb above the free tropospheric values). Above the inversion the concentrations of all of the measured gases gradually decline toward background levels by ~1700 masl. In profile 2 (Figure 4-15) just to the SW of the main gas field (Figure 4-14), CH_4 and NO_2 are very high and ozone is somewhat higher than in profile 1. The enhanced concentrations are mixed up to ~1800 masl consistent with the lack of strong low altitude temperature inversion. Profiles 3 and 4, measured well away from the gas field, have higher O_3 and much lower concentrations of the other measured gases. This picture is consistent with significant photochemical O_3 production occurring as the O_3 precursors are dispersed across the basin.

On February 2 a profile in the gas field (profile 1 – Figures 4-16 - 4-17) shows a strong, shallow inversion with a top at ~1625 masl with strongly enhanced gas concentrations. Just above this

inversion is a very shallow layer with even higher levels of CH_4 and extremely high NO_2 with a significant dip in O_3 indicating titration by NO and conversion to NO_2. This is in contrast to profile 2 just to the west of the gas field (Figure 4-17) where a similar inversion structure has enhanced ozone but NO_2 levels are lower. Ozone below the inversion is also higher than in the gas field reaching ~100 ppb. Profile 3 to the NW of the gas field has a well-mixed layer below the inversion with O_3 of ~100 ppb again indicative of continuing O_3 production as precursors move out of the gas field.

Profiles on February 4 (not shown) have generally well-mixed conditions through a somewhat deeper boundary layer that extends up to 1800 masl in several profiles. For all six profiles on this day O_3 mixing ratios in the boundary layer are over 100 ppb. On February 5 the profiles all have well defined temperature inversion with a top at or just above 1600 masl (Figure 4-19). The trace constituents are well-mixed in the layer. Ozone is above 100 ppb, but somewhat different from the other days as O_3 is highest near the natural gas field exceeding 120 ppb (profiles 3 and 4). All the profiles show a gradual decrease of the trace gas measured concentrations including O_3 up to ~1850 masl. This layer above the lower sharp inversion layer is a characteristic in most of the profiles obtained by the aircraft and represents mixing out of the lowest surface layer into a gradient layer above.

4.4.3 Evidence of Bonanza Power Plant Plume in Vertical Profiles

Profile 4 on February 2 (Figure 4-17) and Profiles 1 and 3 on February 5 (Figure 4-19), as well as on February 4 (not shown), show clear evidence of a plume from the coal-fired Bonanza Power Plant, with enhancements in CO_2, CO, and NO_2 but with low CH_4 and a corresponding depletion in O_3. The power plant plumes were encountered in relatively close proximity to the power plant (~10-16 km). The low CH_4 along with lower O_3 are a clear indication that this plume did not originate from surface sources within the boundary layer. The depression of the O_3 mixing ratio below the tropospheric background measured outside the plume is a clear indication of O_3 titration by the power plant emitted NO. A buoyant plume of emissions from the power plant, whose stack height is at 182 m above ground level, or 1715 masl, is lofted above the 1600-1700 masl inversion layer, and remains above the inversion in a layer that varies in height between 1800 and 1950 masl. This is also shown in photographs taken from the aircraft during the campaign, which clearly show the buoyant plume from the plant above the hazy inversion layer below (Figure 4-20). We conclude that it is unlikely that the power plant emissions contributed significantly to the pollution observed at the surface during this strong temperature inversion event.

Figure 4-20. Photograph taken from the aircraft of the Bonanza Power Plant and its plume rising above the inversion layer on February 2, 2013.

4.5 Flask Samples from Aircraft

Discrete whole air samples were collected in glass flasks aboard the aircraft throughout the seven flights of 2013. Flask samples were also collected in the previous year, in February 2012. Here we present measurements of the whole air collected in flasks in both years, which were analyzed by NOAA's Global Monitoring Division (GMD) in Boulder, CO. In both years, flask samples were also measured at the University of Colorado's Institute of Arctic and Alpine Research (INSTAAR) for additional non-methane hydrocarbons (NMHC), and here we present a subset of that data from 2013. The locations of flask samples over the Uinta Basin in both years are shown in Figure 4-21, along with point sources of possible emissions and oil and gas wells. The 2013 flasks were preferentially sampled near Horsepool, while in 2012 more uniform sampling was achieved.

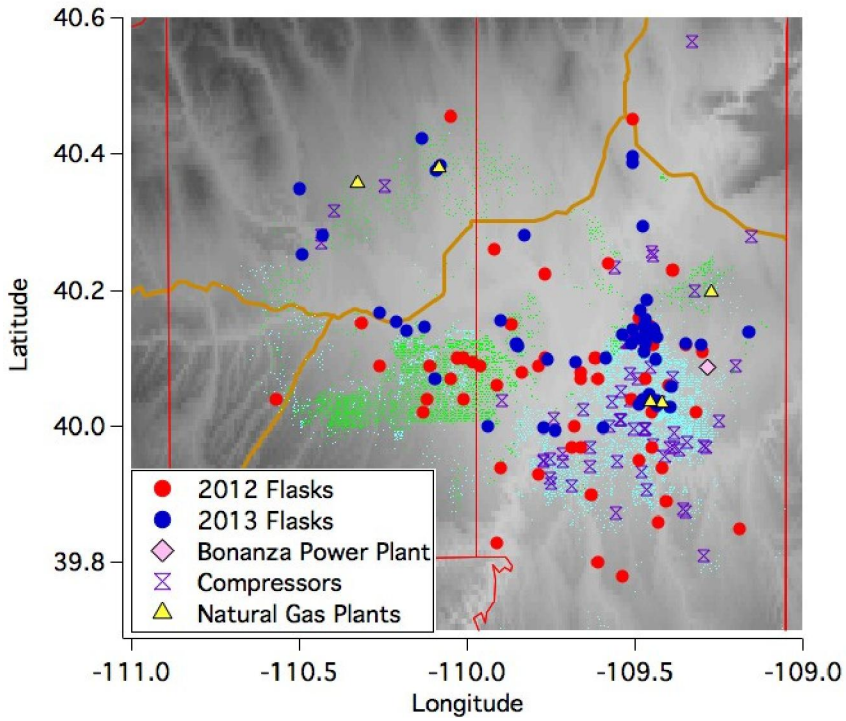

Figure 4-21. Location of flask samples collected in 2012 (red) and 2013 (blue) over the Uinta Basin. Gas wells are indicated in light blue and oil wells in green.

4.5.1 Comparison of Flask Sample Measurements in 2013 and 2012

Figure 4-22 (panels 1-5) shows the measurements of light hydrocarbons that are components of raw natural gas as they correlate with CH_4 in air samples collected in flasks aboard the aircraft in 2012 (gray) and 2013 (blue, red, yellow or green according to the location of the sample collection). Mole fractions of propane (C_3H_8), n-butane (n-C_4H_{10}), n-pentane (n-C_5H_{12}), isopentane (i-C_5H_{12}), and benzene (C_6H_6) show high correlation with CH_4 in both years. Figure 4-22 (bottom right panel) also shows the relationship between CO and CH_4 measured in flask samples in each year; these gases are less well correlated, as discussed in the previous section for the continuous data. As seen in the continuous data (Figure 4-5), CO is more enhanced per unit CH_4 in the SW quadrant of the basin (green). Figure 4-23 shows 2013 measurements of several additional hydrocarbons in the same flasks (from University of Colorado's INSTAAR), all showing correlation with CH_4 and significant enhancements. Some hydrocarbons show higher enhancements per unit CH_4 in the NW and SW quadrants (green and yellow), over the oil field, than in the NE and NW (red and blue), over the gas field. All species were present in significantly higher concentrations in 2013 compared with 2012, most likely because of the shallow layer in which emissions were trapped in 2013 and the lack of winds flushing the basin. In 2012, boundary layer heights were between 500 and 1000 m above ground level during the campaign, while in 2013 the emissions were trapped in a boundary layer of only 100-300 meters.

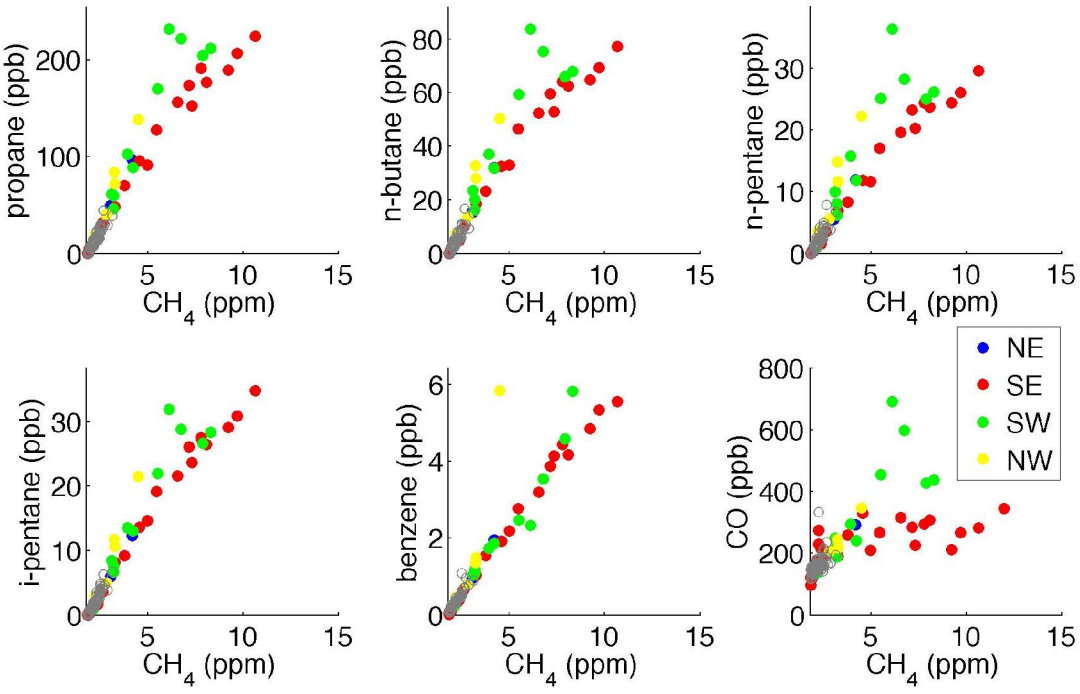

Figure 4-22. Measurements of light hydrocarbons (first five panels) and CO (bottom right) plotted against CH_4 mole fraction from air samples collected in flasks over the Uinta Basin in 2013 (blue, red, green or yellow based on quadrant) and 2012 (gray). All data from NOAA/GMD.

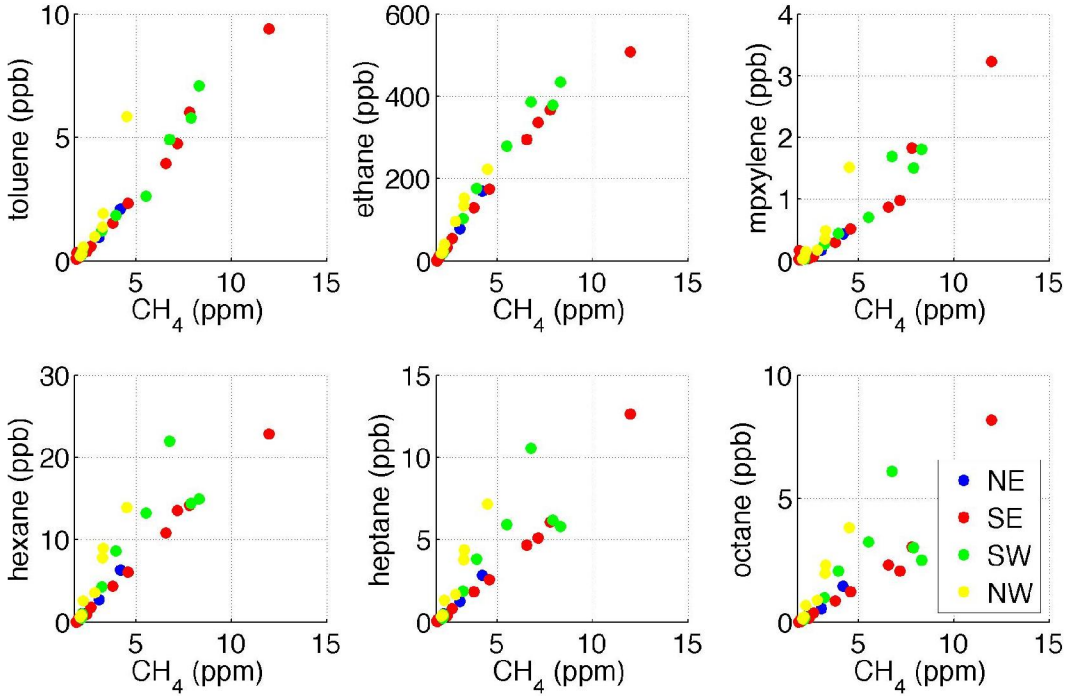

Figure 4-23. Measurements of heavier hydrocarbons in flasks collected aboard the aircraft, January 31 - February 7, 2013, colored by quadrant (CH_4 from NOAA/GMD and NMHC from CU INSTAAR).

4.6 Conclusions

Continuous measurements of O_3, CH_4, CO, CO_2, and NO_2 along with periodic flask measurements during seven aircraft flights between January 31 and February 7, 2013 present an unprecedented picture of both the horizontal and vertical distribution of key atmospheric constituents across the Uinta Basin. With optimal conditions for enhanced O_3 production during the winter of 2013, the relationship between precursor emission sources and O_3 production across the basin was established. Highest concentrations of CH_4 and related non-methane hydrocarbons and NO_2 were observed over the natural gas field in the SE portion of the basin. Longer-lived gases such as CH_4, CO, and CO_2 were more uniformly dispersed across most of the basin and were significantly elevated above background levels. These results suggest that the natural gas field is the likely primary source of O_3 precursor emissions. High O_3 mixing ratios were often seen well away from the gas field itself, strongly indicating ongoing photochemical production as precursors are dispersed across the basin. The strongest enhancements were seen in a relatively shallow surface layer with a strong temperature inversion with a top near 1650±50 masl. There was a gradient layer above this inversion with elevated constituent mixing ratios that gradually declined to near tropospheric background values between 1800 – 1900 masl. Even in the SW sector (over the oil production field), where very high CO values were found on all flights, O_3 was not higher than in other locations. O_3 was

positively correlated with CO over the Basin (Figure 4-11) as might be expected when the CO source is associated with combustion where NO, a primary O_3 precursor, is also emitted. In the SW sector, however, high NO_2 was not generally measured with the very high CO found in this sector and there was no indication of additional O_3 formation.

The highest values of CO measured during the flights were in the SW sector over the region of oil production in Duchesne County. No other constituents measured in this sector showed values elevated above those seen in other parts of the basin. In particular, there was no indication of additional O_3 production seen in conjunction with these very high CO values. Neither high CO_2 nor NO_2 values accompanied these high CO amounts. Correlation plots between CO and other constituents often showed a much different relationship in the SW quadrant, over the oil field, than seen in the other portions of the basin. No immediate source was identified for the strong CO emissions, but the signature of a high CO to CO_2 enhancement ratio indicates a source with inefficient combustion, possibly from the pump jack engines operating in the oil field.

A number of profiles in relatively close proximity (~16 km) to the Bonanza power plant encountered a layer of enhanced CO, CO_2 and NO_2 but with no enhancement in CH_4 and slightly depleted O_3 at an altitude of 1800 – 1900 masl. This composition of trace gas levels was a clear indication of transit through the Bonanza power plant plume. Visual identification of the plume, the altitude of the plume based on the stack height and plume rise, and its composition were clear indicators that the plume had risen through the strong inversion layer. There was also no sign of mixing of the plume from above the inversion back downward to the surface where it could contribute to O_3 production within the geographical boundaries of the study .

4.7 References

Bishop, G. A., and D. H. Stedman, 2008. A decade of on-road emissions measurements, *Environmental Science & Technology*, *42*(5), 1651-1656.

Karion, A., C. Sweeney, S. Wolter, T. Newberger, H. Chen, A. Andrews, J. Kofler, D. Neff, and P. Tans, 2013. Long-term greenhouse gas measurements from aircraft, *Atmos. Meas. Tech.*, *6*(3), 511-526.

Miller, J. B., et al., 2012. Linking emissions of fossil fuel CO_2 and other anthropogenic trace gases using atmospheric (CO_2)-C-14, *J. Geophys. Res.-Atmos.*, *117*.

Peischl, J., et al., 2013. Quantifying sources of methane using light alkanes in the Los Angeles basin, California, *Journal of Geophysical Research: Atmospheres*, n/a-n/a.

Turnbull, J. C., et al., 2011. Assessment of fossil fuel carbon dioxide and other anthropogenic trace gas emissions from airborne measurements over Sacramento, California in spring 2009, *Atmos. Chem. Phys.*, *11*(2), 705-721.

Wunch, D., P. O. Wennberg, G. C. Toon, G. Keppel-Aleks, and Y. G. Yavin, 2009. Emissions of greenhouse gases from a North American megacity, *Geophys. Res. Lett.*, *36*, 5.